Magnetic Resonance Imaging 57 (2019) 118–123

Contents lists available at ScienceDirect

Magnetic Resonance Imaging

journal homepage: www.elsevier.com/locate/mri

Original contribution

Sampling arterial input function (AIF) from peripheral arteries: Comparison of a temporospatial-feature based method against conventional manual method

Xiaowan Li[a], Christopher C. Conlin[a], Stephen T. Decker[b], Nan Hu[c], Michelle Mueller[d], Lillian Khor[e], Christopher Hanrahan[a], Gwenael Layec[b], Vivian S. Lee[f], Jeff L. Zhang[a,*]

[a] Department of Radiology and Imaging Sciences, University of Utah, 729 Arapeen Drive, Salt Lake City, UT, United States
[b] School of Public Health and Health Sciences, University of Massachusetts Amherst, Amherst, Massachusetts
[c] Division of Epidemiology, University of Utah, 295 Chipeta Way, Salt Lake City, UT, United States
[d] Division of Vascular Surgery, University of Utah, 30 N 1900 E, Salt Lake City, UT, United States
[e] Division of Cardiovascular Medicine, University of Utah, 30 N 1900 E, Salt Lake City, UT, United States
[f] Verily Life Sciences, 355 Main St, Cambridge, MA, United States

ARTICLE INFO

Keywords:
Arterial input function
Peripheral artery disease
Connected component analysis
Calf muscles
Magnetic resonance imaging

ABSTRACT

It is often difficult to accurately localize small arteries in images of peripheral organs, and even more so with vascular abnormality vasculatures, including collateral arteries, in peripheral artery disease (PAD). This poses a challenge for manually sampling arterial input function (AIF) in quantifying dynamic contrast-enhanced (DCE) MRI data of peripheral organs. In this study, we designed a multi-step screening approach that utilizes both the temporal and spatial information of the dynamic images, and is presumably suitable for localizing small and unpredictable peripheral arteries. In 41 DCE MRI datasets acquired from human calf muscles, the proposed method took < 5 s on average for sampling AIF for each case, much more efficient than the manual sampling method; AIFs by the two methods were comparable, with Pearson's correlation coefficient of 0.983 ± 0.004 (p-value < 0.01) and relative difference of 2.4% ± 2.6%. In conclusion, the proposed temporospatial-feature based method enables efficient and accurate sampling of AIF from peripheral arteries, and would improve measurement precision and inter-observer consistency for quantitative DCE MRI of peripheral tissues.

1. Introduction

Peripheral artery disease (PAD) in the lower extremity often impairs the performance of calf muscles, thus reducing patient's walking capability [1–3]. DCE MRI has shown promise in noninvasively mapping regional perfusion of the calf muscles [4–7], which could reflect muscle function and also help better understand muscle dysfunction in PAD patients. One critical step in quantifying DCE MRI data is to sample arterial input function (AIF) from a major artery in the field of view [8–20]. However, to sample AIF in calf images can be challenging, because the peripheral arteries in the calf are typically small. In addition, the presence of PAD often alters the peripheral vasculature by narrowing the original arteries and re-growing collateral arteries at new locations [7]. With these features of peripheral arteries, the implementation of conventional manual method would be more challenging, and take even longer processing time than for other locations, such as the abdominal aorta or ventricle.

Multiple methods have been proposed for automatically sampling AIF, with the most popular one being population-averaged AIF. Averaging multiple AIFs may eliminate most artifacts, but at the same time neglect some real features [21,22] that pertain to individual subjects, particularly PAD patients where artery abnormalities are common and spatially variable. Another innovative method is to estimate AIF based on reference tissues for which contrast enhancement parameters are relatively stable [23,24], and in most previous applications, skeletal muscles were chosen as the reference tissue. This is not

Abbreviations: AIF, arterial input function; ABI, ankle-brachial index; CCA, connected component analysis; DCE, dynamic contrast enhanced; FLASH, fast low angle shot; FOV, field of view; FWHM, full width at half maximum; GFR, glomerular filtration rate; PAD, peripheral artery disease; PD, proton density; ROI, region of interest; SE, standard error; S_{max}, Maximum magnitude of the first-pass peak; SNR, signal-to-noise ratio; STD, standard deviation; TE, echo time; TR, repetition time; TTP, time to peak

* Corresponding author at: Radiology Research, University of Utah, 729 Arapeen Drive, Salt Lake City, UT 84108, United States.
E-mail address: lei.zhang@hsc.utah.edu (J.L. Zhang).

https://doi.org/10.1016/j.mri.2018.11.017
Received 24 August 2018; Received in revised form 19 November 2018; Accepted 21 November 2018

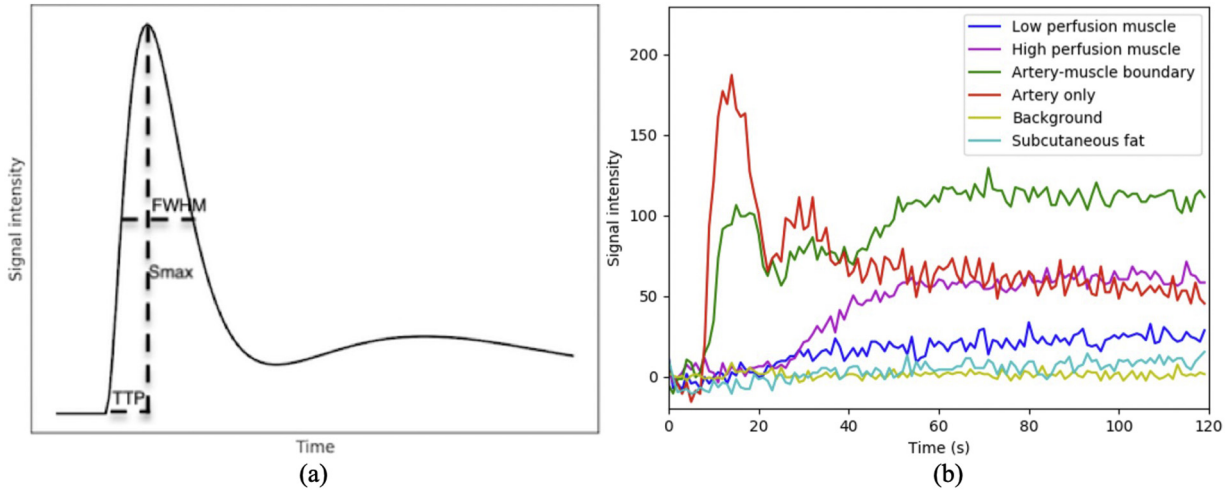

Fig. 1. (a) The well-recognized temporal features for arterial contrast enhancement, including low time to peak (TTP), high first-pass peak (S_{max}), low full width at half maximum (FWHM). (b) Representative signal versus time curves of the different tissue types from exercise-stimulated DCE MRI. For best display effect, baselines of all the curves were aligned to a same level.

feasible for our application, because calf muscles are the tissue of interest. Yet multiple other studies have explored to identify arterial voxels based on the temporal characteristics of their contrast enhancement curves [8,16,25–27]. Such characteristics include early time-to-peak (TTP) [16,25–28], high first-pass peak (S_{max}) [16,25–27,29], low full width at half maximum (FWHM) [8,25–28], and high level of a multi-variable parameter $M = S_{max}/(TTP \times FWHM)$ [26,28]. While spatial or anatomic information was also used in identifying arteries in multiple organs including brain [25], heart [27], breast, and liver [16], none of previous studies succeeded in combining both temporal and spatial features of DCE MRI data in sampling AIF.

In this study, we designed an automatic AIF sampling method that identifies arterial voxels using a multi-step screening approach based on both the temporal and spatial information of the dynamic images. The performance of the proposed method was assessed by comparing it against the manual-sampling method in DCE MRI data acquired from both healthy and PAD subjects.

2. Materials and methods

2.1. DCE MRI of human calf muscles

This study was approved by the local Institutional Review Board (IRB), and we collected overall 41 DCE MRI datasets from 16 human subjects (13 healthy subjects: 41.2 ± 5.2 years, weight 78.1 ± 4.3 kg, height 1.73 ± 0.02 m, 3 females; 3 PAD patients: 63.0 ± 1.2 years, weight 69.7 ± 3.9 kg, height 1.74 ± 0.07 m, 1 female, ankle-brachial index (ABI) 0.73 ± 0.06). With CT angiography, artery stenosis was found in distal superficial femoral artery, posterior tibial artery, and iliac and proximal popliteal arteries for the three PAD patients, respectively. Prior to the MRI scan, written informed consent was obtained from each subject. Each scan was performed on a 3 T MRI scanner (Tim Trio; Siemens Medical Solutions, Erlangen, Germany), with the subject in a supine and feet-first position. A 4-channel flex coil was wrapped around the subject's calf. To reduce leg motion in the imaging, the imaged leg was fixed to the scanner table by one strap over the thigh and the other over the coil. To stimulate calf perfusion, the subject was instructed to perform plantar-flexion exercise with the leg to be imaged in the scanner. The exercise was to push a loaded pedal within a range of motion imposed by the set-up (~13 cm) at a frequency of 1 Hz [30]. Different exercise protocols (weight and duration) were used: 14 scans with a load of 4 lb for 3 min, 8 scans 8 lb for 3 min, 8 scans 16 lb for 3 min, and 11 scans exercised till exhaustion (start with 4 lb with increment of 2 lb per minute). Five seconds before the exercise ended, 0.05 mmol/kg gadoteridol (Prohance; Bracco) was injected intravenously at a rate of 5 ml/s, followed by injection of 20 ml saline at the same rate. Immediately after the exercise ended, dynamic imaging started for an axial slice at the thickest level of the calf, using a 2D saturation-recovery prepared turbo fast low angle shot (FLASH) sequence: delay time 300 ms, repetition time (TR) 527 ms, echo time (TE) 1.42 ms, flip angle 15°, slice thickness 10 mm, matrix 128 × 128, field of view (FOV) 160 × 160 mm, and temporal resolution 1 s/frame [18].

For post-processing, the acquired data were transferred to a personal computer with MATLAB (MathWorks, Natick, MA). Under the guidance of a musculoskeletal radiologist, a user with 10 years' experience in DCE MRI processing identified visible peripheral arteries such as anterior tibial, peroneal, and posterior tibial arteries in the FOV, and manually sampled the voxels from at least one of the three arteries. Caution was taken to avoid partial volume artifacts. Signals of the sampled voxels were averaged, and the resulting signal vs. time curve was considered as the reference.

2.2. Automated sampling of AIF

The method starts with a preliminary screening of arterial voxel *candidates* based on the general pattern of their signal enhancements, and then a further ranking based on a key temporal feature of contrast-enhancement signals. To eliminate partial volume artifact, we identified the relatively large regions in the selected voxels with connected component analysis (CCA), followed by a final trimming step.

2.2.1. Selecting temporal feature of arterial contrast enhancement

The following temporal features have been reported to be characteristic of arterial contrast enhancement: short TTP [16,25–28], high S_{max} [16,25–27], low FWHM [8,25–28], and high M value [26,28], where $M = S_{max}/(TTP \times FWHM)$, as graphically demonstrated in Fig. 1(a) and also in representative signals from our calf-muscle data (Fig. 1(b)). While all the temporal features agree with the principle of tracer kinetics [31], estimation of the different parameters from real noisy data can suffer from different degrees of propagated error. In the following procedure, we determined which of the features would most reliably identify arterial regions in real DCE MRI images with noise. For each of the 41 data, the four parameters (TTP, S_{max}, FWHM, and M) were estimated for all voxels. Specifically, signal vs. time curve for each voxel was first interpolated from 1 s/frame to 0.1 s/frame with a cubic

interpolation. For the interpolated curve, we first identified its highest peak as maximal signal S_{max}; if the peak width at the level of 80% of S_{max} was < 3 s, we treated the peak as a spike due to noise and excluded the voxel from further analysis. For the highest peak (presumably the first-pass peak) of each included curve, we computed TTP, FWHM and M value, and selected the 50 curves (and thus voxels) with the lowest TTP, the highest S_{max}, the lowest FWHM, or the highest M value, respectively. We counted the number of voxels that were identified by both the manual sampling method and the above ranking approach, and then divided the voxel number by the overall number of the manually sampled voxels, or "recall ratio" [32]. This recall ratio was then averaged across all the 41 datasets. Higher recall ratio for a feature indicates that the feature is more characteristic of arterial signal enhancement. The feature with the highest recall ratio was used in ranking the voxels in our proposed method below. Note that for this comparison procedure we did not need an independent set of data, because our goal here was not to train a model based on the temporal metrics, but simply to compare the different metrics.

2.2.2. Identifying arterial voxels based on both temporal and spatial features

In this section, we propose an approach for automatically sampling AIF from DCE MRI data. The approach identifies the arterial voxels by utilizing both their temporal enhancement and the spatial information. As the result of the above comparison, we chose to use the temporal metric S_{max} for ranking the voxels. The approach starts with a preliminary screening based on contrast-enhancement pattern, followed by a more stringent S_{max}-based ranking. Then connected component analysis (CCA) was used to identify the relatively large artery regions without partial volume artifact.

Step 1: Pre-select candidate voxels with detectable contrast enhancement. This pre-selection aims to include voxels fully or partially occupied by blood vessels, and to exclude voxels of pure muscle, background or fat (Fig. 1(b)). Specifically, signals were averaged over a short period at three time points: baseline, peak, and tail. A voxel is pre-selected, if its signal curve fulfills a simple criterion: the peak level is higher than the tail level, which is further higher than the baseline level; both the signal differences should be larger than the noise level, as estimated by the standard deviation (STD) of the signals in the period of 2 to 3 min post-contrast.

Step 2: Rank the candidate voxels to identify the ones with the highest S_{max}. Note that to account for voxels with high S_{max} from other factors (e.g. noisy fat voxels, or muscle voxels containing some vessels), the number of pixels selected in this step (N1) should be set to be larger than the estimated number of true arterial voxels (N2).

Step 3: Identify large artery regions using connected components analysis (CCA) [33]. CCA groups the selected voxels (from Step 2) into multiple connected components based on the locations of the voxels. Similar to Step 2, in customizing the method for a specific application, the number of the selected regions should be larger than the number of predicted arterial regions in the field of view.

Step 4: Re-rank the candidate voxels in the detected large arteries to identify the N2 voxels with the highest S_{max}. In Steps 2 and 3, more voxels (N1 > N2) or regions than expected were intentionally kept, to make sure the major arteries are included. This Step 4 would 'trim' off the voxels on the boundary of an arterial region. Note that Steps 2, 3 and 4 interleave the use of the temporal and spatial criteria in "filtering" the voxels.

For our application of calf muscles, the axial slice at the level of the thickest calf contains 3 major arteries (anterior tibial, peroneal, and posterior tibial artery), with an overall area of 30–40 mm^2. Such area corresponds to 20–30 voxels in our imaging (FOV 160 × 160 mm and matrix 128 × 128). Hence, we set the number of candidate voxels N1 in Step 2 as 50 and the number of arterial regions in Step 3 as 4. In the final step, we set the number of pure-artery voxels N2 as 10 to minimize partial volume artifact. How a proper value for N1 was determined is explained in Appendix.

To evaluate the performance of the proposed method, we computed the Pearson's correlation coefficients (r) [34] and the relative difference (d) between the arterial signal curves sampled by the proposed method and the manually sampled ones. High level of r and low level of d indicate high similarity of two curves and thus high performance of the proposed method. Both the metrics were averaged across the 41 datasets, and are expressed as mean ± standard error (SE). To evaluate the inter-observer variability of the manual sampling method, a second user manually sampled AIF for the same datasets. For each dataset, we computed the Pearson's correlation coefficient and the relative difference between the arterial signal curves sampled by the two users.

3. Results

3.1. Characteristic features of arterial contrast-enhancement

Across the 41 DCE MRI datasets, 95.5% ± 1.7% of the reference voxels were among the 50 voxels with the highest S_{max}. For the other parameters TTP, FWHM and M value, the percentages were 34.5% ± 5.1%, 33.9% ± 5.9% and 79.5% ± 3.7%, respectively. Based on this preliminary study, it was determined that in manual sampling of AIF in axial images of calf, a high S_{max} was the most consistently distinctive feature among the four features, in differentiating artery from other tissues in a same field of view.

3.2. Performance of the automatic AIF sampling approach

The proposed method successfully sampled AIFs from all 41 datasets, without user assistance. On average, the proposed method took about 5 s, while the manual sampling took 10–20 min for each dataset. For a representative case, we show the intermediate result after each step of the proposed method in Fig. 2.

With the proposed method, all the three major calf arteries (peroneal, anterior tibial, and posterior tibial artery) were detected in 11 out of the 41 cases. Of the 41 cases, peroneal artery was identified in 39 cases, anterior tibial artery in 22 cases, and posterior tibial artery in 25 cases. This finding agrees with the fact that on the imaging level of the calf, the peroneal artery is the thickest branch of all the three arteries.

Averaged across the 41 datasets, Pearson's correlation coefficient (r) and the relative difference (d) between the signal curves from the proposed and the reference method were 0.983 ± 0.004 (p-value < 0.01) and 2.4% ± 2.6%, respectively (Table 1). Fig. 3 shows the two worst AIFs sampled by the proposed automated method, one with the lowest r value 0.87 and the other with the highest d value 43%. Between the different groups (healthy versus PAD, and different exercise intensities), we did not detect a significant difference in terms of the correlation coefficients or the relative differences. Fig. 4 shows two sets of example AIFs, one from a healthy subject (26 years old) and the other from a PAD patient (61 years old), which differed much in their magnitude but were both sampled by the proposed method with high accuracy. While the proposed automatic method has zero inter-observer variability, Pearson's correlation coefficient and the relative difference between the manually sampled signal curves by the two users were 0.953 ± 0.014 and −2.2% ± 1.6%, respectively.

4. Discussion

Sampling of AIF is a crucial step in quantitative processing of DCE MRI data, but is challenging for some peripheral organs. The presence of PAD could make it even more challenging. In our acquired data of

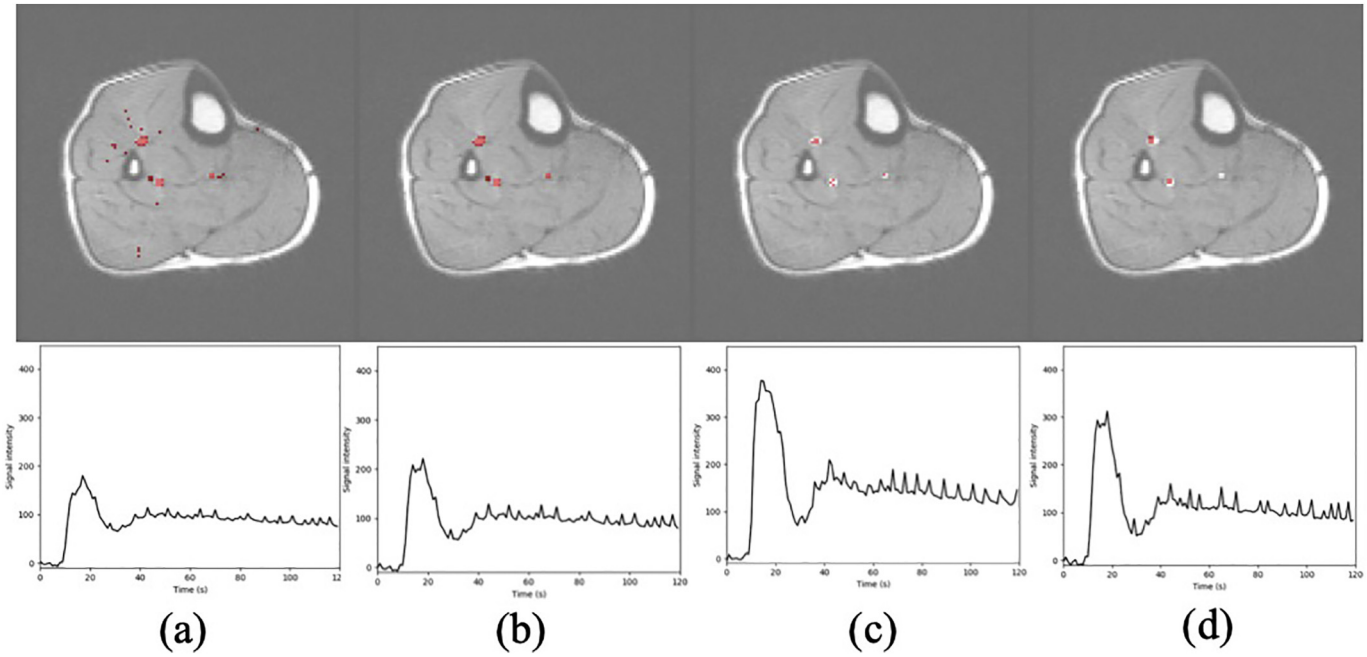

Fig. 2. Representative example to demonstrate the proposed AIF sampling process. In Step 1 (not shown here) all voxels with contrast enhancement were selected. Then the voxels with the highest S_{max} (a) were identified in Step 2. The large arterial regions (b) were selected by CCA in Step 3 and were further trimmed to remove boundary voxels (c). For comparison, the manual reference voxels and AIF are shown in (d). For this example, the correlation coefficient of the enhancement curves from each of the three arteries against its manual reference was 0.914, 0.977, 0.998, and the relative difference was −18.9%, −11.4%, 8.4%, respectively.

Table 1
Pearson's correlation coefficient and relative difference between the signal curves from the proposed method and the manual sampling method for all the 41 data.

Cases	Pearson's correlation coefficient	Relative difference	Cases	Pearson's correlation coefficient	Relative difference
1	0.995	−19.3%	23	0.994	−37.8%
2	0.996	−11.4%	24	0.998	8.4%
3	0.998	−13.0%	25	0.990	5.6%
4	0.997	25.7%	26	0.925	−19.6%
5	1.000	0.9%	27	0.971	−8.0%
6	0.985	−3.3%	28	0.996	−0.8%
7	0.981	16.5%	29	0.999	19.6%
8	0.990	9.6%	30	0.984	42.5%
9	0.992	2.1%	31	0.999	−3.3%
10	0.970	3.2%	32	0.974	14.8%
11	0.994	21.3%	33	0.999	8.3%
12	0.993	0.3%	34	0.990	13.5%
13	0.999	−5.4%	35	0.985	2.2%
14	0.960	5.1%	36	0.987	10.5%
15	0.983	22.8%	37	0.993	−16.0%
16	0.868	−13.4%	38	0.893	−12.0%
17	0.995	−37.8%	39	0.998	−5.6%
18	0.991	5.3%	40	0.964	9.7%
19	0.990	38.3%	41	0.996	0.9%
20	0.992	25.0%			
21	0.980	−0.2%	Mean	0.983	2.4%
22	0.997	−6.4%	Standard error	0.004	2.6%

calf muscles, the number of arterial voxels sampled manually in PAD patients by an experienced user was noticeably lower than that in healthy subjects (2.3 ± 0.49 vs. 3.4 ± 0.26). In this study, we proposed a multi-step screening method for sampling AIF. For the 41 DCE MRI data acquired from human calf muscles, the proposed method produced AIFs that highly resembled the manually-sampled ones.

One major decision in our proposed method was which of previously reported temporal feature should be used for voxel ranking. According to tracer kinetic principles, all the four features (high S_{max}, low TTP, low FWHM, high M value) are characteristic of arterial contrast enhancement. However, to accurately estimate the different parameters from noisy enhancement curves is challenging by different degrees. Time to peak (TTP) is computed as the difference between bolus arrival time and peak time. Accurate estimation of bolus arrival time can be challenging, and its difference between arterial and high-perfusion voxels is sometimes small. Estimation of FWHM requires interpolation or reliable curve fitting first. The parameter M involves all the other three parameters. Of the four parameters, S_{max} takes the least computation effort for its estimation. In addition, with S_{max} as a sampling criterion, the voxels with partial volume artifact (e.g. those of small vessels or on the boundary of large arteries) can be directly excluded. The potential advantage of S_{max} over other parameters was verified in a preliminary comparison with our DCE MRI data. However, this should not preclude future studies in designing new screening method using some combination of multiple temporal features.

Instead of screening the voxels with temporal feature only, our method also incorporates spatial feature (i.e. the area of the selected regions in Step 3), and interleaves the use of temporal and spatial criteria in a multi-step procedure: coarse screening with temporal pattern, the first ranking with S_{max}, CCA for large regions, and the second ranking with S_{max}. This multi-step interleaved manner could effectively include the true arterial voxels, and at the same time discard the non- or partial-artery voxels. Anatomic information was also used in determining the numbers of voxel candidates in each step. For example, with the estimate of 20–30 artery voxels in our calf slice, in Step 2 of ranking we kept the 50 voxels (Fig. A.1) with highest S_{max}, making sure to include all arteries in FOV, and then in Step 4 of trimming, kept only about 10 voxels to avoid partial volume artifact. A good estimate of the overall arterial area in the FOV would increase the speed and performance of the proposed method. By the careful design that utilizes both temporal and spatial information, our method is made fully automatic, advantageous over the clustering-based methods that require pre-cropping or pre-segmentation [25,27,35] and are usually computationally inefficient [26,28,35]. Note that, because PAD could alter the vasculature of the calf, we did not use the pre-defined location of the

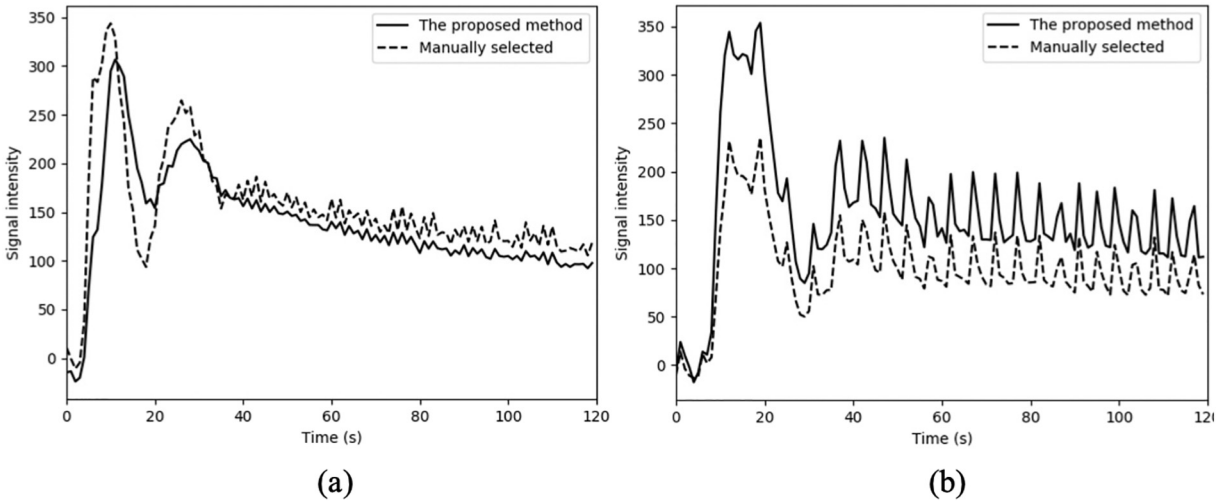

Fig. 3. The two datasets with the largest difference between sampled arterial signals by the proposed method and by the manual sampling. (a) The lowest Pearson's correlation coefficient 0.87. (b) The highest relative difference 43%; the signals sampled by the manual method were lower, presumably due to its partial volume artifact.

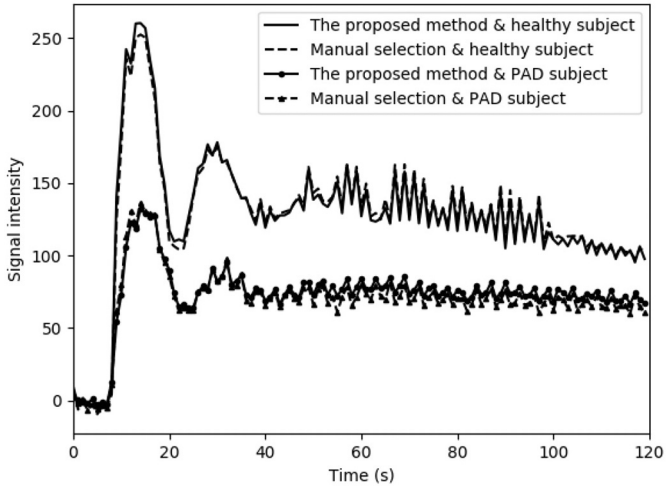

Fig. 4. AIFs successfully sampled for a young healthy subject and for an aged PAD patient. As the proposed method is based on a ranking approach, its performance was not affected by the magnitude of the signals.

arteries as in the previous studies [16,25,27], but instead estimate the cross-sectional area of the arteries in assisting AIF sampling.

This study has several limitations. First, some combinations of the different temporal features could outperform S_{max} in identifying the arterial voxel candidates. This will be explored in future study. Second, in evaluating the performance of the proposed method, we compared it against conventional manual sampling method, which may suffer from some errors. An ideal validation is to compare against contrast concentrations in sampled arterial blood, or alternatively, to perform simulation where true AIF is known. Third, we did not apply the sampled AIFs for quantifying tissue perfusion parameters. In model-based optimization approach, we expect that the error in AIF would be proportionally propagated into tissue perfusion estimates. Fourth, the proposed method was tested on a small group of human subjects, and only 3 of them were PAD patients. Test on more human subjects is needed for future study. Fifth, the proposed method does not correct for motion artifact. Some PAD patients may experience involuntary leg twitching, so as a future work, the method can be improved by incorporating some image registration algorithm.

In conclusion, by utilizing temporal and spatial features in a multi-step interleaved manner, the proposed method effectively identified arterial input functions that highly resembled those manually sampled by expert in leg arteries. Its applicability in other peripheral organs should be tested in future studies.

Funding

This work was supported by the: NIDDK [grant number: R01 DK109349] and NHLBI [grant number: R01 HL135242].

Appendix A. Number of candidate voxels (N1) selected in S_{max} ranking (Step 2)

To determine a proper value for N1, as a preparatory step we repeated Step 2 with different N1 values from 10 to 100 (with 10 as interval), and computed the resulted "recall ratio" [32] as the number of manually sampled voxels in the candidate voxels over the number of all manually sampled voxels. The number N1 should be high enough to include as many arterial voxels as possible (i.e. high recall ratio), but at the same time should be low enough to exclude non-artery voxels. Fig. A.1 shows the resulted recall ratio from the various N1 values. The recall ratio increased from 72.3% ± 3.6% at N1 of 10, to 95.5% ± 1.7% at N1 of 50; further increase of N1 to 100 led to small increase in recall ratio to 98.2% ± 1.1%. Based on this analysis, we set N1 at 50, a number about 2 times of the estimated arterial voxels.

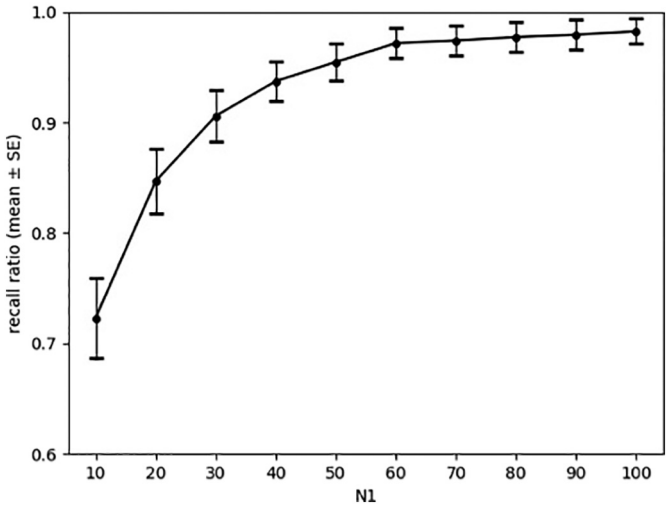

Fig. A.1. The relationship between the number (N1) of candidate voxels (the voxels with the highest S_{max} in Step 2) and the resulted recall ratio. Increase in N1 would lead to increase in recall ratio, but the latter plateaus at N1 of 50–60.

References

[1] McDermott MM. Lower extremity manifestations of peripheral artery disease: the pathophysiologic and functional implications of leg ischemia. Circ Res 2015;116(9):1540–50.

[2] McDermott MM, Greenland P, Liu K, Guralnik JM, Criqui MH, Dolan NC, et al. Leg symptoms in peripheral arterial disease: associated clinical characteristics and functional impairment. JAMA 2001;286(13):1599–606.

[3] McDermott MM, Guralnik JM, Tian L, Ferrucci L, Liu K, Liao Y, et al. Baseline functional performance predicts the rate of mobility loss in persons with peripheral arterial disease. J Am Coll Cardiol 2007;50(10):974–82.

[4] Isbell DC, Epstein FH, Zhong X, DiMaria JM, Berr SS, Meyer CH, et al. Calf muscle perfusion at peak exercise in peripheral arterial disease: measurement by first-pass contrast-enhanced magnetic resonance imaging. J Magn Reson Imaging 2007;25(5):1013–20.

[5] Versluis B, Dremmen MH, Nelemans PJ, Wildberger JE, Schurink G-W, Leiner T, et al. Dynamic contrast-enhanced MRI assessment of hyperemic fractional microvascular blood plasma volume in peripheral arterial disease: initial findings. PLoS One 2012;7(5):e37756.

[6] Lutz AM, Weishaupt D, Amann-Vesti BR, Pfammatter T, Goepfert K, Marincek B, et al. Assessment of skeletal muscle perfusion by contrast medium first-pass magnetic resonance imaging: technical feasibility and preliminary experience in healthy volunteers. J Magn Reson Imaging 2004;20(1):111–21.

[7] Venkatesh BA, Nauffal V, Noda C, Fujii T, Yang PC, Bettencourt J, et al. Baseline assessment and comparison of arterial anatomy, hyperemic flow, and skeletal muscle perfusion in peripheral artery disease: the Cardiovascular Cell Therapy Research Network "Patients with Intermittent Claudication Injected with ALDH Bright Cells"(CCTRN PACE) study. Am Heart J 2017;183:24–34.

[8] Calamante F, Morup M, Hansen LK. Defining a local arterial input function for perfusion MRI using independent component analysis. Magn Reson Med 2004;52(4):789–97.

[9] Sun Y, Schmidt NO, Schmidt K, Doshi S, Rubin JB, Mulkern RV, et al. Perfusion MRI of U87 brain tumors in a mouse model. Magn Reson Med 2004;51(5):893–9.

[10] Morris ED, VanMeter JW, Tasciyan TA, Maisog J, Zeffiro T. Automated determination of the arterial input function for quantitative MR perfusion analysis. Proc Int Soc Magn Reson Med 2000;740.

[11] Zhang JL, Rusinek H, Chandarana H, Lee VS. Functional MRI of the kidneys. J Magn Reson Imaging 2013;37(2):282–93.

[12] Sourbron SP, Michaely HJ, Reiser MF, Schoenberg SO. MRI-measurement of perfusion and glomerular filtration in the human kidney with a separable compartment model. Invest Radiol 2008;43(1):40–8.

[13] Cutajar M, Mendichovszky I, Tofts P, Gordon I. The importance of AIF ROI selection in DCE-MRI renography: reproducibility and variability of renal perfusion and filtration. Eur J Radiol 2010;74(3):e154–60.

[14] Rahim Zadeh H, Kazerooni AF, Deevband MR, Saligheh Rad H. Arterial input function selection in DSC-MRI of brain tumors using differential evaluation clustering method. ISMRM; 2017. p. 4381.

[15] Yankeelov TE, Lepage M, Chakravarthy A, Broome EE, Niermann KJ, Kelley MC, et al. Integration of quantitative DCE-MRI and ADC mapping to monitor treatment response in human breast cancer: initial results. Magn Reson Imaging 2007;25(1):1–13.

[16] Chen J, Yao J, Thomasson D. Automatic determination of arterial input function for dynamic contrast enhanced MRI in tumor assessment. International conference on medical image computing and computer-assisted intervention. Springer; 2008. p. 594–601.

[17] Barrett T, Brechbiel M, Bernardo M, Choyke PL. MRI of tumor angiogenesis. J Magn Reson Imaging 2007;26(2):235–49.

[18] Vivier P-H, Storey P, Rusinek H, Zhang JL, Yamamoto A, Tantillo K, et al. Kidney function: glomerular filtration rate measurement with MR renography in patients with cirrhosis. Radiology 2011;259(2):462–70.

[19] Mendichovszky I, Cutajar M, Gordon I. Reproducibility of the aortic input function (AIF) derived from dynamic contrast-enhanced magnetic resonance imaging (DCE-MRI) of the kidneys in a volunteer study. Eur J Radiol 2009;71(3):576–81.

[20] Mendichovszky I, Pedersen M, Frøkiær J, Dissing T, Grenier N, Anderson P, et al. How accurate is dynamic contrast-enhanced MRI in the assessment of renal glomerular filtration rate? A critical appraisal. J Magn Reson Imaging 2008;27(4):925–31.

[21] Wang Y, Huang W, Panicek DM, Schwartz LH, Koutcher JA. Feasibility of using limited-population-based arterial input function for pharmacokinetic modeling of osteosarcoma dynamic contrast-enhanced MRI data. Magn Reson Med 2008;59(5):1183–9.

[22] Sabuncu MR, Balci SK, Shenton ME, Golland P. Image-driven population analysis through mixture modeling. IEEE Trans Med Imaging 2009;28(9):1473–87.

[23] Heisen M, Fan X, Buurman J, ter Haar Romeny B. Effects of reference tissue AIF derived from low temporal resolution DCE-MRI data on pharmacokinetic parameter estimation. ISMRM-ESMRMB joint annual meeting 2010. - Sweden, Stockholm, Stockholm. 2010. p. 4802.

[24] Yankeelov TE, Luci JJ, Lepage M, Li R, Debusk L, Lin PC, et al. Quantitative pharmacokinetic analysis of DCE-MRI data without an arterial input function: a reference region model. Magn Reson Imaging 2005;23(4):519–29.

[25] Peruzzo D, Bertoldo A, Zanderigo F, Cobelli C. Automatic selection of arterial input function on dynamic contrast-enhanced MR images. Comput Methods Programs Biomed 2011;104(3):e148–57.

[26] Mouridsen K, Christensen S, Gyldensted L, Ostergaard L. Automatic selection of arterial input function using cluster analysis. Magn Reson Med 2006;55(3):524–31.

[27] Jacobs M, Benovoy M, Chang LC, Arai AE, Hsu LY. Evaluation of an automated method for arterial input function detection for first-pass myocardial perfusion cardiovascular magnetic resonance. J Cardiovasc Magn Reson 2016;18:17.

[28] Yin J, Sun H, Yang J, Guo Q. Automated detection of the arterial input function using normalized cut clustering to determine cerebral perfusion by dynamic susceptibility contrast-magnetic resonance imaging. J Magn Reson Imaging 2015;41(4):1071–8.

[29] Brunner G, Bismuth J, Nambi V, Ballantyne CM, Taylor AA, Lumsden AB, et al. Calf muscle perfusion as measured with magnetic resonance imaging to assess peripheral arterial disease. Med Biol Eng Comput 2016;54(11):1667–81.

[30] Layec G, Trinity JD, Hart CR, Kim S-E, Groot HJ, Le Fur Y, et al. In vivo evidence of an age-related increase in ATP cost of contraction in the plantar flexor muscles. Clin Sci 2014;126(8):581–92.

[31] Tofts PS. Modeling tracer kinetics in dynamic Gd-DTPA MR imaging. J Magn Reson Imaging 1997;7(1):91–101.

[32] Goutte C, Gaussier E. A probabilistic interpretation of precision, recall and F-score, with implication for evaluation. European conference on information retrieval. Springer; 2005. p. 345–59.

[33] Vincent L. Morphological grayscale reconstruction in image analysis: applications and efficient algorithms. IEEE Trans Image Process 1993;2(2):176–201.

[34] Benesty J, Chen J, Huang Y, Cohen I. Pearson correlation coefficient. Noise reduction in speech processing. Springer; 2009. p. 1–4.

[35] Murase K, Kikuchi K, Miki H, Shimizu T, Ikezoe J. Determination of arterial input function using fuzzy clustering for quantification of cerebral blood flow with dynamic susceptibility contrast-enhanced MR imaging. J Magn Reson Imaging 2001;13(5):797–806.